Nanoscale Discrimination between Toxic and Non-Toxic Protein Misfolded Oligomers with Tip-Enhanced Raman Spectroscopy

Cristiano D'Andrea, Antonino Foti,#, Maximilien Cottat,§, Martina Banchelli, Claudia Capitini, Francesco Barreca, Claudio Canale, Marella de Angelis, Annalisa Relini, Onofrio M. Maragò, Roberto Pini, Fabrizio Chiti, Pietro G. Gucciardi,* and Paolo Matteini**

Dr. Cristiano D'Andrea, Dr. Maximilien Cottat, Dr. Martina Banchelli, Dr. Marella de Angelis, Prof. Roberto Pini, Dr. Paolo Matteini
IFAC-CNR, Institute of Applied Physics "Nello Carrara", National Research Council, Via Madonna del Piano 10, I-50019 Sesto Fiorentino, Italy
E-mail: p.matteini@ifac.cnr.it
Dr. Antonino Foti, Dr. Onofrio O. Maragò, Dr. Pietro G. Gucciardi
IPCF-CNR, Institute for Chemical and Physical Processes, National Research Council, Viale F. Stagno D'Alcontres 37, I-98158 Messina, Italy
E-mail: gucciardi@ipcf.cnr.it
Dr. Claudia Capitini, Prof. Fabrizio Chiti
Department of Biomedical Experimental and Clinical Sciences, University of Florence, Viale Morgagni 50, I-50134 Firenze, Italy
E-mail: fabrizio.chiti@unifi.it
Dr. Francesco Barreca,
Department of MIFT, University of Messina, Viale F. Stagno d'Alcontres 31, I-98166 Messina, Italy
Dr. Claudio Canale
Department of Physics, University of Genoa, Via Dodecaneso 33, I-16146 Genova, Italy.
Prof. Annalisa Relini
Department of Chemistry and Industrial Chemistry, University of Genoa, Via Dodecaneso 31, I-16146 Genova, Italy

now at LPICM, Ecole Polytechnique, CNRS, 91128 Palaiseau France
§ now at Laboratoire des Technologies et de la Microélectronique, CNRS, 17 avenue des martyrs (CEA-LETI), 38054 Grenoble Cedex, France

Keywords: TERS, nanoscale, biomolecules, Alzheimer's disease, amyloid

Highly toxic protein misfolded oligomers associated with neurological disorders such as Alzheimer's and Parkinson's diseases are nowadays considered primarily responsible for promoting synaptic failure and neuronal death. Unravelling the relationship between structure and neurotoxicity of protein oligomers appears pivotal in understanding the causes of the pathological process, as well as in designing novel diagnostic and therapeutic strategies tuned

toward the earliest and pre-symptomatic stages of the disease. Here we benefit from tip-enhanced Raman spectroscopy (TERS) as a surface-sensitive tool with spatial resolution on the nanoscale, to inspect the spatial organization and surface character of individual protein oligomers from two samples formed by the same polypeptide sequence and different toxicity levels. TERS provides direct assignment of specific amino acid residues that are exposed to a large extent on the surface of toxic species and buried in non-toxic oligomers. These residues, thanks to their outward disposition, might represent structural factors driving the pathogenic behaviour exhibited by protein misfolded oligomers, including affecting cell membrane integrity and specific signaling pathways in neurodegenerative conditions.

1. Introduction

The accumulation of aberrant forms of aggregated peptides or proteins as amyloid fibrils is at the basis of a large number of human pathologies, ranging from neurodegenerative disorders, such as Alzheimer's, Parkinson's, Creutzfeldt-Jacob's and Huntington's diseases, to non-neuropathic amyloidoses, including type II diabetes and systemic amyloidosis.[1] As far as Alzheimer's disease (AD) is concerned, it is now widely accepted that oligomeric forms of the β-amyloid (Aβ) peptide, generated during the early stages of the pathology as a key event of the overall process of amyloid fibril formation, initiate cellular processes causing the impairment of the cognitive functions.[2,3] Importantly, the molecular events leading to the formation of these species are supposed to appear 10 to 20 years before the symptoms become evident.[4] Studies aimed at unravelling the relationship between structure and neurotoxicity of misfolded oligomers are thus pivotal in gaining insights into the pathological process, as well as in designing novel diagnostic and therapeutic strategies tuned toward the earliest and pre-symptomatic stages of the disease.[5-7]

Plasmon-enhanced spectroscopies rely on the peculiar optical properties of noble metal nanostructures (localized plasmon resonances) permitting to enhance the optical responses of molecules in their close proximity.[8] A main representative of plasmon-enhanced spectroscopies is surface-enhanced Raman spectroscopy (SERS) in which metal nanostructures are exploited to enhance the Raman scattering of nearby molecules up to 10 orders of magnitude.[9] As a result, identification of trace amounts of molecular species becomes feasible. This has recently inspired a number of studies aimed at the quantification and structural characterization of physiological quantities of proteins and other biomolecules.[10-17]

In tip-enhanced Raman spectroscopy (TERS) the high sensitivity of SERS is combined with the nanoscale spatial resolution of scanning probe microscopy (SPM).[18-22] TERS exploits the high-localized EM field enhancement on a sharp metallized tip to achieve compositional and structural information from the surface of nanosized samples.[23-25] Nowadays this technique is perceived as a valuable candidate for complementing conventional techniques used to determine the structures of biological macromolecules such as X-ray crystallography or nuclear magnetic resonance (NMR) spectroscopy, offering unique information at the nanometer level from single supramolecular entities and aggregates.[26-29] The group of Zenobi showed, in 2013, the combined use of Scanning Tunnelling Microscopy (STM) and TERS to identify single Aβ peptide nanotapes.[30] In this study, the spectroscopic information provided by TERS permitted the unambiguous assignment of the structure of the protein assemblies preliminary imaged by STM. Deckert and co-workers investigated by TERS individual insulin fibrils, retrieving their amino acid residue composition.[31] The authors evidenced the conformational variety along the fibril by mapping alternating hydrophobic and hydrophilic domains and providing valuable information on the sites active for biological interactions. Recently, Bonhommeau et al., showed *via* TERS the differentiation between the wild type of Aβ fibrils and two synthetic mutants, the latter obtained by substitution of a

specific amino acid in the polypeptide sequence and notably forming toxic oligomers and non-toxic fibrils.[32]

In this work, we take inspiration from the above mentioned achievements to demonstrate the use of TERS in discriminating between two forms of soluble misfolded oligomers formed by the 91-residues N-terminal domain of the *E. coli* protein HypF (HypF-N, **Figure S1**, Supporting Information), denoted as type A and type B, which show the same polypeptide sequence, similar morphology but different abilities to cause cellular dysfunction, with type A oligomers being toxic compared to non-toxic type B species.[6] HypF-N represents a valuable model system as it forms spherical oligomers and amyloid-like fibrils *in vitro* similar to those associated with neurodegenerative diseases.[33,34] In addition, HypF-N oligomers impair cell viability when added to cultured cells or injected into animals, similarly to oligomers found in many amyloid diseases;[35,36] they produce all the effects of the Aβ oligomers associated with Alzheimer's disease at the biochemical, biological and electrophysiological level; importantly, they are stable and maintain their morphological and structural properties even under conditions very different from those that promoted their formation, allowing their detailed study at the structural and biological level.

Our TERS investigation provides compelling evidence of the presence of chemostructural determinants in the case of toxic oligomers, which sheds new light on the mechanism by which they cause cellular impairment. Specifically, we identified specific aminoacid residues that appear exposed on the surface of toxic oligomers while buried in the non-toxic forms, with obvious implications for the elucidation of the structural factors responsible for cell toxicity at the single residue level.

2. Results and Discussion

Raman spectra of the toxic type A (**Figure 1**, red line) and non-toxic type B (**Figure 1**, blue line) HypF-N oligomers were initially acquired. An almost-perfect overlap of the spectra is apparent, that prevents us from discriminating between the two types. After baseline correction and multi-peak fitting of the resulting Raman profiles (inset of **Figure 1**), characteristic vibrational modes were deduced and summarized in **Table 1**.

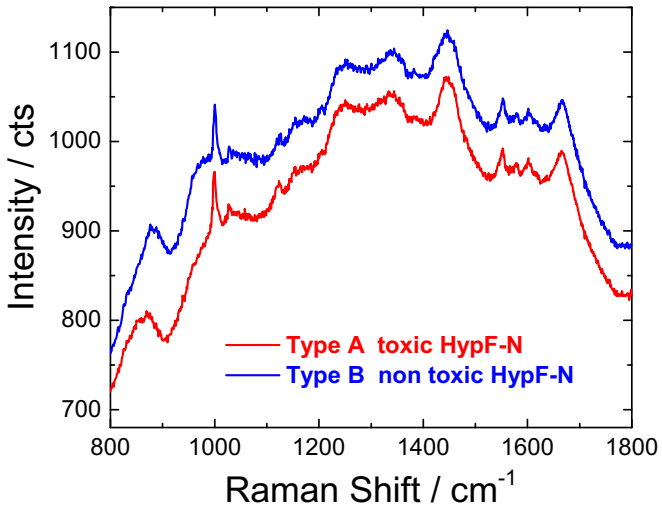

Figure 1. Raman spectra of type A (red line) and type B (blue line) HypF-N oligomers. The spectra are acquired in identical experimental conditions (same excitation power and integration time).

Table 1. Assignment of the main spectral bands of HypF-N oligomers as detected by conventional Raman spectroscopy and TERS.

Raman peak position (cm^{-1})	Mode Assignment	TERS peak position (cm^{-1})
830, 850	Tyr	rare
1003	Phe	1003
1027	Phe	1027
1240	amide III - β-sheet	--
1250-1280	amide III - random coil, α-helix	
1430-1470	CH_2, CH_3 deformations	--
--	His	1500
--	amide II	1520
--	amide II + His	1538
1551	Trp	1550
1576	Trp	1575
1603	Tyr + Phe	1600
1617	Tyr	1620
1635	amide I - random coil	1640 - 1680
1653	amide I - α-helix	
1668	amide I - β-sheet	
1690-1700	amide I - β-turn/random coil	

By comparing the curve-fitting components in the region between 1400 cm^{-1} and 1800 cm^{-1} with the Raman profiles of isolated aromatic amino acids (**Figure S2**, Supporting Information), we were able to assign the peaks at 1551 cm^{-1} and 1576 cm^{-1} to Trp residues, at 1603 cm^{-1} to Tyr and Phe residues and at 1617 cm^{-1} to Tyr side chains.[37]. A broad amide I band covers the 1635-1700 cm^{-1} range, which comprises both α-helix (1653 cm^{-1}) and β-sheet (1668 cm^{-1}) modes, while the 1430-1470 cm^{-1} peak originates from CH_2 and CH_3 deformations.[38,39] Amide III modes contain a β-sheet contribution at 1240 cm^{-1} and another at 1250 - 1280 cm^{-1} including random coils and α-helices.[40] Finally, the Fermi doublet of Tyr can be observed at 830 and 850 cm^{-1}, while 1003 and 1027 cm^{-1} modes are assigned to Phe ring breathing and in-plane ring deformations, respectively.[41,42] The spectral assignments obtained by Raman spectroscopy were used as reference for TERS in the following, in view

of the overlapping peaks usually expected by using an identical excitation wavelength, while being aware that band intensity ratios can be much different.[20,43,44]

AFM measurements on the samples used for the TERS experiments (**Figure S3**, Supporting Information) outlined a distribution of isolated oligomers with globular shape and similar size (type A oligomers: 2.0 ± 0.1 nm height, 15 ± 1 nm width; type B oligomers: 3.5 ± 0.4 nm height, 10 ± 1 nm width). The homogeneous density of the oligomers detected suggests that the procedure used for sample preparation was appropriate enough to prevent clustering or undesired over-aggregation. Three TERS maps of 200×200 nm^2 were acquired from different regions of the samples, collecting 25 nm-stepped spectra, for a total of 64 spectra per map (an exemplary TERS/STM combined map is reported in **Figure S4**, Supporting Information). Considering the dimensions of the inspected species, the step size used in TERS mapping ensures that the signal from each position originates from a different oligomeric unit. A preliminary screening of the acquired TERS spectra consisted in removing those with signals matching the fluorescence background of the gold tip (~ 50%). Further on, spectra with Raman features that were not enough intense to perform a clear assignment of the relative modes (~ 10%) were discarded. Each map provided then an average of 30 selected spectra per map, for a total of 80-90 spectra for both type A and B oligomers resulting from the three investigated maps. We note that the unavailability of more than half of the inspected sites to generate effective TERS signals can be caused by the roughness of the gold-coated supports used to get STM feedback in our experiments. In fact both toxic and non-toxic oligomer distributions resemble the morphology of the underneath surface that is strewn with 90 ± 5 nm large, and 3.8 ± 0.1 nm high adjacent Au domains (**Figure S3**, Supporting Information) with resulting underexposed sample portions, which are hardly accessible to the tip (**Figure S5**, Supporting Information).

Figure 2a,b reports a collection of selected TERS spectra acquired from type A and type B oligomer samples. In spite of the local signal variations that are consequential to the chemical complexity produced by adjacent amino acid residues,[32,45,46] a tentative assignment of the main TERS bands was made based on the Raman spectra (see **Table 1)**. In particular, aromatic ring vibrations are visible at 1003 and 1027 cm^{-1} (Phe) and within the 1550-1620 cm^{-1} range (Trp, Tyr, Phe).[32,44] His ring deformations look like isolated (1500 cm^{-1}) or overlapped with the amide II modes (1538 cm^{-1}).[47] The amide I modes appear at 1640-1680 cm^{-1}[48] in both oligomer spectra. The Tyr doublet at 830-850 cm^{-1} is frequently unnoticeable and limited to type A spectra while the amide III (1220-1280 cm^{-1}) and the CH_2/CH_3 (1430-1470 cm^{-1}) bands are affected by severe fluctuations and will not receive further consideration in this article. On the basis of the above considerations, we focused the analysis on the 980-1050 cm^{-1} and 1490-1710 cm^{-1} regions. Such regions were fitted by a multi-peak Lorentzian fit (**Figure S6**, Supporting Information**)** and the integrated areas of the fitted peaks were plotted in box plots (**Figure S7**, Supporting Information) to highlight the main spectral differences between the two oligomer types.

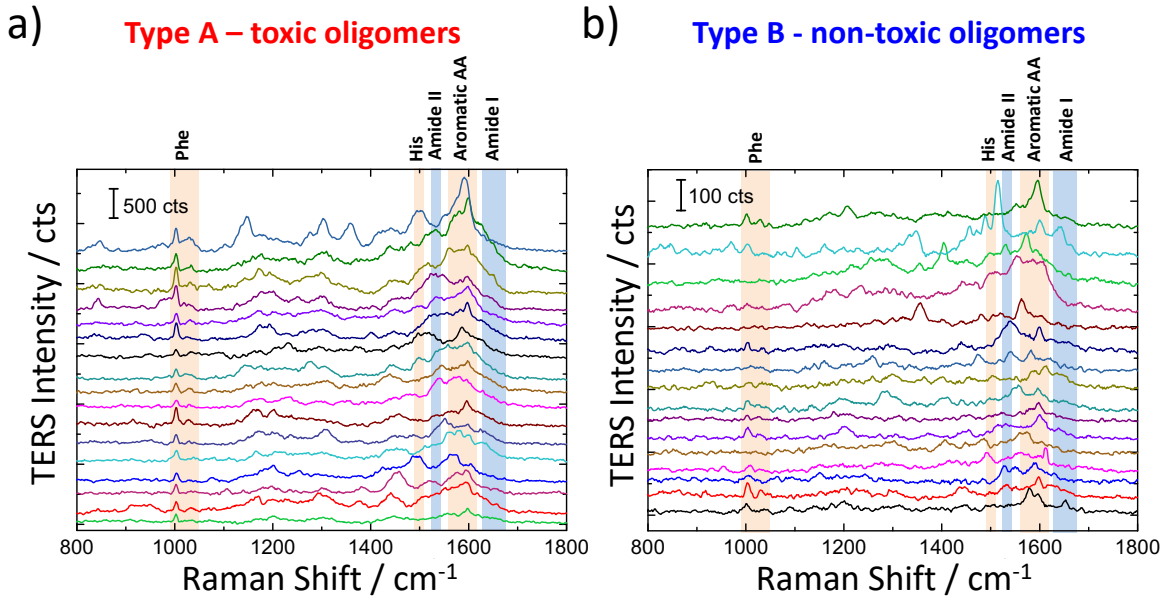

Figure 2. TERS spectra of type A (a) and type B (b) oligomers. The bands used for the analysis are highlighted by coloured boxes: aromatic amino acids and histidines (ligh red

boxes) and amide I and II bands (light blue boxes). All the spectra are acquired in identical experimental conditions (same TERS tip, power, objective, integration time). The background is removed and the spectra are offseted for clarity.

In order to rule out intensity biases due to local fluctuations in the enhancement factor as well as in surface density and local molecular orientation of the samples, which could influence the signal measured from the type A and type B samples, we normalized the intensity of the main peaks in the 1000 – 1030 cm^{-1} and 1500 – 1680 cm^{-1} regions with respect to the corresponding intensity of the Phe mode at 1003 cm^{-1} (I/I_{1003}, **Figure 3**) on a spectrum-by-spectrum basis. This latter mode (as well as the 1027 cm^{-1} mode), in fact, is poorly affected by the environment and frequently used as "internal" reference for the analysis of biological samples.[49,50] We note that the amide I as well as the amide II modes exhibit almost overlapping I/I_{1003} interval values in both type A and type B oligomers and their average values approach the Phe mode at 1003 cm^{-1}. Conversely, the other modes appear largely more intense in type A than in type B spectra. In particular, the His band at 1500 cm^{-1} features a 4-fold larger TERS amplification for type A with respect to type B. Similar considerations hold, as well, for the aromatic ring vibrations in the 1550-1620 cm^{-1} range, which appear much more intense in the toxic type A oligomers. A reduced distance between the TERS tip and these residues is expected to primarily boost their TERS intensity.[51] In fact, because the local electromagnetic field distribution follows an exponential decay with distance from the tip apex,[21,22] a larger signal enhancement of the most accessible residues lying within the range of the hot spot's tip is produced. On the basis of the above observations, we can infer an outer position of His and the aromatic amino acids on the surface of type A oligomer while a buried location of these residues inside the oligomer may be deduced in type B.

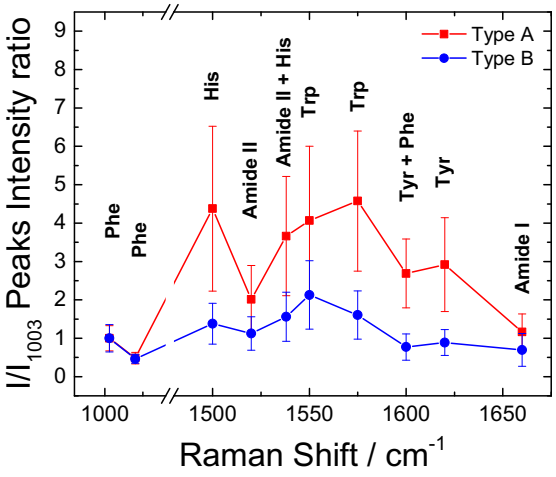

Figure 3. Intensity ratio (I/I_{1003} ±SD) of the integrated areas (calculated by a multi-Lorentzian fit) of the observed TERS peaks in the 1000 – 1030 cm^{-1} and 1500 – 1670 cm^{-1} regions for type A (red squares) and type B (blues circles) oligomers.

A noticeable dispersion in peak amplitudes in the case of type A oligomers, especially occurring for the His mode at 1500 cm^{-1} and for the Trp modes at 1550 and 1575 cm^{-1} (SD ~40%, **Figure 3**, and broad interquartile intervals, **Figure S7,** Supporting Information, were estimated for these modes), which appears less pronounced for the Phe and Tyr modes at 1600 cm^{-1} and at 1620 cm^{-1}, is another main outcome. Signal fluctuations of this entity may be justified by the occurrence of a charge transfer between tip and substrate, which is strictly dependent from the immediate residue/tip contacts.[51] In this context, His and Trp are expected to produce the highest high-end values because of their heterocyclic moieties (*i.e.* imidazole and indole rings) sustaining strong absorbate-surface interactions, which are expected to be weaker in the case of the phenol and phenyl rings of Tyr and Phe.[52-54]

The I_{TypeA}/I_{TypeB} ratio between the mean values of the band fitting areas of TERS modes of type A and type B oligomers provides a quantitative picture of the tendency shown by each oligomeric form to locate certain aminoacid residues on its surface (**Figure 4**). I_{TypeA}/I_{TypeB} values of His and the aromatic amino acid modes around 2 - 3 folds larger for toxic as

compared to non-toxic oligomers were observed. We note that the same ratio as calculated from Raman spectra appears unable to provide a clear discrimination between the two oligomer types as initially perceived (**Figure 1**). These results highlight the superior ability of TERS in probing structural domains specifically located on the surface of the inspected specimen, which, conversely, is not readily accessible by either bulk vibrational spectroscopy or by any other technique.

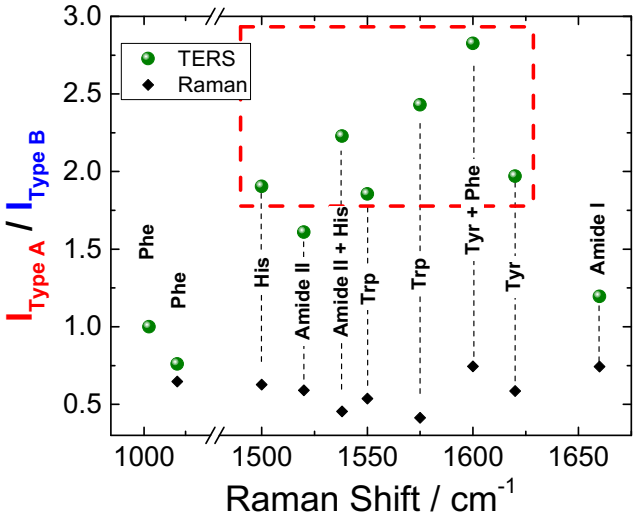

Figure 4. Comparison between the ratios of integrated intensities (I_{TypeA}/I_{TypeB}) obtained by the fit process over TERS (green circles) and Raman (black diamonds) spectra of type A and type B oligomers.

Concerning previous research, several achievements associated a solvent-exposure of specific regions on the surface of misfolded oligomers with their aberrant interactions against cellular components.[1,6,55-59] For instance, in a study on the characterization of two types of $A\beta_{42}$ oligomers showing similar size but different toxicity, it was found that two segments of Aβ (*i.e.* the hydrophobic 16-22 and 30-42 residue regions) were more solvent-exposed in the oligomer showing higher toxicity levels.[58] Toxic and non-toxic forms of α-synuclein oligomers were also found to differently expose hydrophobic regions, in particular a N-

terminus that is required to anchor the toxic species to the membrane, and a β-sheet structure core that inserts into the membrane.[59] Fluorescence data obtained with ANS site-directed labelling with different fluorophores and fluorescence resonance energy transfer (FRET) measurements pointed out to a connection between the toxicity of type A HypF-N oligomers and the higher solvent-exposure of three main hydrophobic regions, which encompass 18-30, 55-65 and 75-87 residues.[6,60] Interestingly, the aromatic residues as well as one of the two His residues (His64) of the HypF-N molecule are wholly located in these regions (**Figure S1**, Supporting Information). Further evidence of the exposure of hydrophobic residues in type A oligomers is given in **Figure S8**, Supporting Information, by contact angle measurements. Thus the intense TERS signals emerging from our investigation in the case of His and the aromatic amino acids in type A species (**Figure 3**) provide a direct confirmation of a peculiar superficial structuring existing on toxic misfolded species that causes cellular dysfunction. Interestingly, the presence of top signals as observed for amino acid residues of toxic species containing reactive side-chains such as imidazole in His and phenol in Tyr (**Figure 4**), is suggestive of the importance of such exposed moieties in neuronal membrane interactions.[61,62]

3. Conclusion

We demonstrated the potential of TERS in identifying characteristic chemostructural elements of protein oligomeric forms associated with amyloid diseases, showing same peptide sequence and different toxicity levels. By exploiting the capabilities of the TERS technique to access the specimen with nanometric resolution, spatial organization and surface character of individual oligomers were carefully inspected. Furthermore, being the TERS response originated from a well localized hot-spot on the tip apex, these evaluations are conferred with quantitative significance. Ultimately, TERS provided a direct assignment of specific amino acid residues exposed to a larger extent on the surface of the toxic species. These residues,

due to their outward disposition, might play a role in the pathogenic behaviour exhibited by toxic oligomers, including affecting cell membrane integrity and specific signaling pathways in neurodegenerative conditions.

4. Experimental Section

Oligomers preparation: HypF-N oligomers were prepared as previously reported.[6] Briefly, toxic (type A) oligomers were obtained by diluting the HypF-N monomer to a final concentration of 48 $\times 10^{-6}$ M in 50 $\times 10^{-3}$ M acetate buffer (pH 5.5) containing 12% (v/v) trifluoroethanol (TFE) and 2 $\times 10^{-3}$ M DTT. To prepare non-toxic (type B) oligomers a similar procedure was used apart from diluting the monomer in 20 $\times 10^{-3}$ M trifluoroacetic acid (pH 1.7) containing 330 $\times 10^{-3}$ M NaCl. The samples were incubated for 4 h at 25 °C. In order to stop the process, the aggregating solution was centrifuged at 16000 g for 10 min followed by 95% removal of the supernatant, which was replaced by the same volume of 7 $\times 10^{-3}$ M potassium phosphate buffer (pH 7.4). Freshly prepared solutions of oligomers kept at 25 °C were used in all the experiments.

Raman experiments: The Raman analysis was performed on drop-casted HypF-N oligomer solutions (20 μL) left drying at room temperature on an aluminium substrate. Raman spectra were acquired by using a Horiba Xplora micro-Raman spectrometer coupled to a 638 nm excitation laser. The backscattering light was collected by a 10×-microscope objective with 0.25 NA (spot diameter ~ 7 μm), and 30 s of acquisition time. Laser power at the sample was 2 mW. Raman data represent an average of a minimum of 10 spectra acquired from different positions of the sample.

TERS experiments: TERS measurements were carried out with a commercial setup (XploRa Nano, Horiba) which couples a Raman micro-spectrometer to a Scanning Probe Microscope (AIST-NT SmartSPM^{TM}-1000) capable to operate in STM, Atomic Force (AFM) or Shear Force (ShFM) microscopy modes (**Figure S9**, Supporting Information). The STM

configuration was chosen for our purposes, in which the oligomers are deposited on a flat metallic surface. The laser beam (λ = 638 nm) used to excite the sample was focused on the tip through a 100× long working distance objective (Mitutoyo, WD 6.0 mm, NA 0.7), in a side-illumination configuration with an angle of θ_{inc} = 60° with respect to the vertical axis. Polarization is set linear and parallel to the tip axis. The backscattered TERS signal was collected by the same objective and driven to the spectrometer. The signal, first dispersed by a grating (1200 lines/mm) was acquired by a Peltier cooled CCD camera (Syncerity, Horiba). The metallic surface consisted of a gold-coated Si substrate (100 nm 99.99% Au on Si wafer, Sigma Aldrich) cleaned by plasma pre-treatment (Harrick Scientific Corp., PDC-002 operated at 60 Hz and 0.2 Torr air) for 5 min and then overnight (16 h) immersed in the HypF-N oligomer solution. The samples were then rinsed in water to remove the unbound molecules, air-dried and finally used for TERS experiments. All the TERS maps were recorded exciting with a 0.1 mW laser power at the sample and acquisition time of 30 s. In order to exclude any contamination of the tip during the experiments, after each map a control measurement was performed on the tip apex with no sample, obtaining only the gold fluorescence background. By comparing the TERS intensity to the reference signal measured when the tip is out of contact, we estimated an enhancement factor $EF \geq 10^5$ (**Figure S10**, Supporting Information).

AFM experiments: The surface morphology of the samples was inspected by tapping mode AFM. Images of gold substrates before and after incubation with toxic or non-toxic HypF-N oligomers were acquired in air using a Dimension 3100 SPM equipped with "G" scanning head (maximum scan size 100 μm) and driven by a Nanoscope IIIa controller, and a Multimode SPM equipped with "E" scanning head (maximum scan size 10 μm) and driven by a Nanoscope V controller (Digital Instruments-Bruker). Single beam uncoated silicon cantilevers (type OMCL-AC160TS, Olympus) were used. The drive frequency was between 270 and 300 kHz and the scan rate was 0.5-1.0 Hz.

Supporting Information
Supporting Information is available from the Wiley Online Library or from the author.

Acknowledgements
C.D'A., M.C, M.B., M.deA., R.P., F.C. and P.M. acknowledge the Tuscany Region within the project "Surface-enhanced Raman spectroscopy for the early diagnosis of Alzheimer's disease SUPREMAL" (PAR FAS 2007- 2013 Action Line 1.1- Action 1.1.2). C.D'A., M.C, M.B., M.deA., R.P. and P.M. acknowledge the European Community within the EuroNanoMed3 ERANET cofund (H2020) project "Surface-enhanced Raman scattering with nanophotonic and biomedical amplifying systems for an early diagnosis of Alzheimer's disease pathology SPEEDY" (ID 221). C.C. thanks the Centre for Misfolding diseases of the University of Cambridge. A.R. thanks Filippo Tramontana for help in AFM measurements. O.M. and P.G.G. acknowledge the project POR SICILIA FERS 2007/2013 Linea 4.1.2A "MEDiterranean NETwork for emerging NAnomaterials MEDNETNA" for financial support.

Received: ((will be filled in by the editorial staff))
Revised: ((will be filled in by the editorial staff))
Published online: ((will be filled in by the editorial staff))

References

[1] F. Chiti, C. M. Dobson, *Annu. Rev. Biochem.* **2017**, *86*, 27.
[2] I. Benilova, E. Karran, B. De Strooper, *Nat. Neurosci.* **2012**, *15*, 349.
[3] A. B. Reiss, H. A. Arain, M. M. Stecker, N. M. Siegart, L. J. Kasselman, *Rev. Neurosci.* **2018**.
[4] D. S. Knopman, S. T. DeKosky, J. L. Cummings, H. Chui, J. Corey-Bloom, N. Relkin, G. W. Small, B. Miller, J. C. Stevens, *Neurology* **2001**, *56*, 1143.
[5] F. Bemporad, F. Chiti, *Chem. Biol.* **2012**, *19*, 315.
[6] S. Campioni, B. Mannini, M. Zampagni, A. Pensalfini, C. Parrini, E. Evangelisti, A. Relini, M. Stefani, C. M. Dobson, C. Cecchi, F. Chiti, *Nat. Chem. Biol.* **2010**, *6*, 140.
[7] O. Klementieva, K. Willen, I. Martinsson, B. Israelsson, A. Engdahl, J. Cladera, P. Uvdal, G. K. Gouras, *Nat. Commun.* **2017**, *8*, 14726.
[8] K. A. Willets, R. P. Van Duyne, *Annu. Rev. Phys. Chem.* **2007**, *58*, 267.
[9] E. C. LeRu, P. G. Etchegoin, *Principles of Surface-Enhanced Raman Spectroscopy: And Related Plasmonic Effects*, Elsevier, Oxford **2009**.
[10] L. Guerrini, R. Arenal, B. Mannini, F. Chiti, R. Pini, P. Matteini, R. A. Alvarez-Puebla, *ACS Appl. Mater. Interfaces* **2015**, *7*, 9420.
[11] M. Cottat, C. D'Andrea, R. Yasukuni, N. Malashikhina, R. Grinyte, N. Lidgi-Guigui, B. Fazio, A. Sutton, O. Oudar, N. Charnaux, V. Pavlov, A. Toma, E. Di Fabnzio, P. G. Gucciardi, M. L. de la Chapelle, *J. Phys. Chem. C* **2015**, *119*, 15532.
[12] B. Fazio, C. D'Andrea, A. Foti, E. Messina, A. Irrera, M. G. Donato, V. Villari, N. Micali, O. M. Marago, P. G. Gucciardi, *Sci. Rep.* **2016**, *6*.
[13] P. Matteini, M. Cottat, F. Tavanti, E. Panfilova, M. Scuderi, G. Nicotra, M. C. Menziani, N. Khlebtsov, M. de Angelis, R. Pini, *Acs Nano* **2017**, *11*, 918.

[14] E. Pazos, M. Garcia-Algar, C. Penas, M. Nazarenus, A. Torruella, N. Pazos-Perez, L. Guerrini, M. E. Vazquez, E. Garcia-Rico, J. L. Mascarenas, R. A. Alvarez-Puebla, *J. Am. Chem. Soc.* **2016**, *138*, 14206.
[15] M. Prochazka, Surface-Enhanced Raman Spectroscopy: Bioanalytical, Biomolecular and Medical Applications. In *Surface-Enhanced Raman Spectroscopy: Bioanalytical, Biomolecular and Medical Applications*, Springer, Switzerland **2016**.
[16] N. Feliu, M. Hassan, E. G. Rico, D. X. Cui, W. Parak, R. Alvarez-Puebla, *Langmuir* **2017**, *33*, 9711.
[17] M. Banchelli, M. de Angelis, C. D'Andrea, R. Pini, P. Matteini, *Sci. Rep.* **2018**, *8*, 1033.
[18] L. Langelueddecke, P. Singh, V. Deckert, *Appl. Spectr.* **2015**, *69*, 1357.
[19] T. Schmid, L. Opilik, C. Blum, R. Zenobi, *Angew. Chem. Int. Ed.* **2013**, *52*, 5940.
[20] N. Kumar, S. Mignuzzi, W. T. Su, D. Roy, *EPJ Tech. Instrum.* **2015**, *2*.
[21] B. Pettinger, K. F. Domke, D. Zhang, G. Picardi, R. Schuster, *Surf. Sci.* **2009**, *603*, 1335.
[22] P. Verma, *Chem. Rev.* **2017**, *117*, 6447.
[23] A. B. Zrimsek, N. H. Chiang, M. Mattei, S. Zaleski, M. O. McAnally, C. T. Chapman, A. I. Henry, G. C. Schatz, R. P. Van Duyne, *Chem. Rev.* **2017**, *117*, 7583.
[24] S. Jiang, Y. Zhang, R. Zhang, C. R. Hu, M. H. Liao, Y. Luo, J. L. Yang, Z. C. Dong, J. G. Hou, *Nat. Nanotechnology* **2015**, *10*, 865.
[25] S. Jiang, X. B. Zhang, Y. Zhang, C. R. Hu, R. Zhang, Y. Zhang, Y. Liao, Z. J. Smith, Z. C. Dong, J. G. Hou, *Light-Science & Applications* **2017**, *6*.
[26] B. R. Wood, M. Asghari-Khiavi, E. Bailo, D. McNaughton, V. Deckert, *Nano Lett.* **2012**, *12*, 1555.
[27] E. Lipiec, R. Sekine, J. Bielecki, W. M. Kwiatek, B. R. Wood, *Angew. Chem. Int. Ed.* **2014**, *53*, 169.
[28] M. Tabatabaei, F. A. Caetano, F. Pashee, S. S. G. Ferguson, F. Lagugne-Labarthet, *Analyst* **2017**, *142*, 4415.
[29] S. Bonhommeau, S. Lecomte, *Chemphyschem* **2018**, *19*, 8.
[30] M. Paulite, C. Blum, T. Schmid, L. Opilik, K. Eyer, G. C. Walker, R. Zenobi, *Acs Nano* **2013**, *7*, 911.
[31] T. Deckert-Gaudig, D. Kurouski, M. A. B. Hedegaard, P. Singh, I. K. Lednev, V. Deckert, *Sci. Rep.* **2016**, *6*, 33575.
[32] S. Bonhommeau, D. Talaga, J. Hunel, C. Cullin, S. Lecomte, *Angew. Chem. Int. Ed.* **2017**, *56*, 1771.
[33] F. Chiti, M. Bucciantini, C. Capanni, N. Taddei, C. M. Dobson, M. Stefani, *Protein Sci.* **2001**, *10*, 2541.
[34] A. Relini, S. Torrassa, R. Rolandi, A. Gliozzi, C. Rosano, C. Canale, M. Bolognesi, G. Plakoutsi, M. Bucciantini, F. Chiti, M. Stefani, *J. Mol. Biol.* **2004**, *338*, 943.
[35] B. Mannini, E. Mulvihill, C. Sgromo, R. Cascella, R. Khodarahmi, M. Ramazzotti, C. M. Dobson, C. Cecchi, F. Chiti, *ACS Chem. Biol.* **2014**, *9*, 2309.
[36] R. Cascella, S. Conti, B. Mannini, X. Y. Li, J. N. Buxbaum, B. Tiribilli, F. Chiti, C. Cecchi, *Biochim. Biophys. Acta* **2013**, *1832*, 2302.
[37] A. Rygula, K. Majzner, K. M. Marzec, A. Kaczor, M. Pilarczyk, M. Baranska, *J. Raman Spectrosc.* **2013**, *44*, 1061.
[38] E. Podstawka, Y. Ozaki, L. M. Proniewicz, *Appl. Spectrosc.* **2004**, *58*, 570.
[39] N. C. Maiti, M. M. Apetri, M. G. Zagorski, P. R. Carey, V. E. Anderson, *J. Am. Chem. Soc.* **2004**, *126*, 2399.
[40] E. Podstawka, Y. Ozaki, L. M. Proniewicz, *Appl. Spectrosc.* **2004**, *58*, 1147.
[41] B. Sjoberg, S. Foley, B. Cardey, M. Enescu, *Spectrochim. Acta A Mol. Biomol. Spectrosc.* **2014**, *128*, 300.
[42] G. Y. Zhu, X. Zhu, Q. Fan, X. L. Wan, *Spectrochim. Acta A Mol. Biomol. Spectrosc.* **2011**, *78*, 1187.

[43] D. Kurouski, T. Postiglione, T. Deckert-Gaudig, V. Deckert, I. K. Lednev, *Analyst* **2013**, *138*, 1665.
[44] C. Blum, T. Schmid, L. Opilik, S. Weidmann, S. R. Fagerer, R. Zenobi, *J. Raman Spectrosc.* **2012**, *43*, 1895.
[45] C. Blum, L. Opilik, J. M. Atkin, K. Braun, S. B. Kaemmer, V. Kravtsov, N. Kumar, S. Lemeshko, J.-F. Li, K. Luszcz, T. Maleki, A. J. Meixner, S. Minne, M. B. Raschke, B. Ren, J. Rogalski, D. Roy, B. Stephanidis, X. Wang, D. Zhang, J.-H. Zhong, R. Zenobi, *J. Raman Spectrosc.* **2014**, *45*, 22.
[46] C. C. vandenAkker, T. Deckert-Gaudig, M. Schleeger, K. P. Velikov, V. Deckert, M. Bonn, G. H. Koenderink, *Small* **2015**, *11*, 4131.
[47] T. Deckert-Gaudig, E. Kaemmer, V. Deckert, *J. Biophotonics* **2012**, *5*, 215.
[48] D. Kurouski, T. Deckert-Gaudig, V. Deckert, I. K. Lednev, *Biophys. J.* **2014**, *106*, 263.
[49] V. Kocherbitov, J. Latynis, A. Misiunas, J. Barauskas, G. Niaura, *J. Phys. Chem. B* **2013**, *117*, 4981.
[50] M. F. Rosario-Alomar, T. Quinones-Ruiz, D. Kurouski, V. Sereda, E. B. Ferreira, L. De Jesus-Kim, S. Hernandez-Rivera, D. V. Zagorevski, J. Lopez-Garriga, I. K. Lednev, *J. Phys. Chem. B* **2015**, *119*, 1265.
[51] V. Sereda, I. K. Lednev, *Appl. Spectrosc.* **2017**, *71*, 118.
[52] E. J. Bjerneld, F. Svedberg, P. Johansson, M. Kall, *J. Phys. Chem. A* **2004**, *108*, 4187.
[53] T. Deckert-Gaudig, E. Rauls, V. Deckert, *J. Phys. Chem. C* **2010**, *114*, 7412.
[54] A. Singha, S. Dasgupta, A. Roy, *Biophys. Chem.* **2006**, *120*, 215.
[55] H. Olzscha, S. M. Schermann, A. C. Woerner, S. Pinkert, M. H. Hecht, G. G. Tartaglia, M. Vendruscolo, M. Hayer-Hartl, F. U. Hartl, R. M. Vabulas, *Cell* **2011**, *144*, 67.
[56] R. Krishnan, J. L. Goodman, S. Mukhopadhyay, C. D. Pacheco, E. A. Lemke, A. A. Deniz, S. Lindquist, *Proc. Natl. Acad. Sci. USA* **2012**, *109*, 11172.
[57] B. Bolognesi, J. R. Kumita, T. P. Barros, E. K. Esbjorner, L. M. Luheshi, D. C. Crowther, M. R. Wilson, C. M. Dobson, G. Favrin, J. J. Yerbury, *ACS Chem. Biol.* **2010**, *5*, 735.
[58] A. R. A. Ladiwala, J. Litt, R. S. Kane, D. S. Aucoin, S. O. Smith, S. Ranjan, J. Davis, W. E. Van Nostrand, P. M. Tessier, *J. Biol. Chem.* **2012**, *287*, 24765.
[59] G. Fusco, S. W. Chen, P. T. F. Williamson, R. Cascella, M. Perni, J. A. Jarvis, C. Cecchi, M. Vendruscolo, F. Chiti, N. Cremades, L. M. Ying, C. M. Dobson, A. De Simone, *Science* **2017**, *358*, 1440.
[60] C. Capitini, J. R. Patel, A. Natalello, C. D'Andrea, A. Relini, J. A. Jarvis, L. Birolo, A. Peduzzo, M. Vendruscolo, P. Matteini, C. M. Dobson, A. De Simone, F. Chiti, *Chem Comm.* **2018**, DOI: 10.1039/C8CC03446J.
[61] D. G. Smith, G. D. Ciccotosto, D. J. Tew, K. Perez, C. C. Curtain, J. F. Boas, C. L. Masters, R. Cappai, K. J. Barnham, *J. Alzheimers Dis.* **2010**, *19*, 1387.
[62] C. Wallin, S. B. Sholts, N. Osterlund, J. H. Luo, J. Jarvet, P. M. Roos, L. Ilag, A. Graslund, S. Warmlander, *Sci. Rep.* **2017**, *7*, 14423.